

Connectivity of Confined Dense Networks: Boundary Effects and Scaling Laws

Justin P. Coon, Carl P. Dettmann, and Orestis Georgiou

Abstract

In this paper, we study the probability that a dense network confined within a given geometry is fully connected. We employ a cluster expansion approach often used in statistical physics to analyze the effects that the boundaries of the geometry have on connectivity. To maximize practicality and applicability, we adopt four important point-to-point link models based on outage probability in our analysis: single-input single-output (SISO), single-input multiple-output (SIMO), multiple-input single-output (MISO), and multiple-input multiple-output (MIMO). Furthermore, we derive diversity and power scaling laws that dictate how boundary effects can be mitigated (to leading order) in confined dense networks for each of these models. Finally, in order to demonstrate the versatility of our theory, we analyze boundary effects for dense networks comprising MIMO point-to-point links confined within a right prism, a polyhedron that accurately models many geometries that can be found in practice. We provide numerical results for this example, which verify our analytical results.

Index Terms

Connectivity, percolation, outage, MIMO, diversity, power scaling.

I. INTRODUCTION

Multihop relay networks have received a lot of attention recently due to their ability to improve coverage and, thus, capacity in a geographical sense. Many of these networks – such as mesh networks, vehicular networks, wireless sensor networks, and *ad hoc* networks – possess commonality insofar as the number and distribution of nodes in the network is often random. A considerable amount of research on random networks has been conducted in the past (see, e.g., [1]–[3]). From a communications perspective, it is of paramount importance to understand the connectivity properties of such networks. This understanding can lead to improved protocols and network deployment methodologies in practice [4].

In recent years, researchers have adopted and adapted a number of techniques from the physics and mathematical communities to study connectivity in random networks. Perhaps the most directly applicable theory that has been employed is that of continuum percolation [5], owing to its long and rich history of use in describing particle clustering in statistical physics and fluid dynamics [6]–[10]. In particular, percolation theory is concerned with the emergence of a single large connected component (possibly in addition to other finite connected components) in a large (typically unbounded) graph, and dictates the minimum node density – which is known as the *critical node density* – required to obtain such a component. The links to network connectivity are obvious. Percolation theory has been applied in recent years to identify and analyze power management techniques that can be used to ensure network connectivity [11], [12]. It has also been used to demonstrate the benefits that node cooperation gives to improving connectivity [13]–[16]. Further applications of the general theory of percolation (including bond and site percolation) can be found in studies of network resilience [17], hybrid networks (i.e., random networks with a regular element) [18], coverage and connectivity in wireless sensor networks [19] (a direct application of [9]), and the information theoretic capacity of networks [20].

While the benefits of using percolation theory to explore asymptotic connectivity issues in random networks is clear, the theory does not directly address the question: what is the probability that *all* nodes in the network are connected? This question falls under the heading of *full connectivity* rather than

percolation. The answer to this question is, of course, related to a number of parameters, such as the fading environment, the path loss model, the node density, and the geometry in which the network resides. Many researchers have studied full connectivity, typically in some asymptotic regime. Two particular network models have been popularized for the study of full connectivity: the *extended network model* and the *dense network model*. The former relates to the case where the node density is finite and the network area is large, whereas the latter specifies a finite network area with a high node density (see, e.g., [21] and the references therein).

With regard to extended networks, in [13], [16], the authors assume a *unit disk connection model*¹ and give conditions on the path loss exponent for which full connectivity can be achieved in one-dimensional and two-dimensional networks. For dense networks, a number of scaling laws have been published. For example, in [22], the authors derive a power scaling law that ensures full connectivity is achieved *almost surely* as the number of nodes in the network tends to infinity. In [23], scaling laws are given for the number of nearest neighbors (i.e., connections per node) that are required to achieve full connectivity asymptotically in the number of nodes. Related results are given in [24] for sectorized networks.

More practical connection models (as opposed to the unit disk model) have also been considered in the literature [25]–[30]. Specifically, the authors of [26], [27] considered a probabilistic connection model whereby log-normal shadowing was incorporated into the path loss model. Both 1-connectivity and k -connectivity² were considered in those papers. In [29], the authors considered the effects of fast fading (in particular, Rayleigh and Rician fading) on full connectivity in dense networks, and derived expressions for the node isolation probability for several cases of interest. Note that this probability effectively defines a first order approximation of the full-connectivity probability for dense networks, a point that we will elaborate upon later. Finally, the authors of [30] have recently studied connectivity with respect to the decay properties of a general *pair-connectedness probability function*.

The various contributions related to dense networks typically specify some geometry in which the network resides. These geometries are commonly taken to be squares or circles in two dimensions. One aspect that is common to virtually all of this research is that boundary effects are neglected in the interest of deriving a simple elegant result. *In this paper, we show that such effects should not, in general, be neglected since they tend to dictate performance (in terms of the full-connectivity probability) in the high density limit*³. We provide a constructive explanation of this assertion through the application of a novel cluster expansion model, first developed in [31], [32], which admits an accurate first order inhomogeneous approximation in the limit of large density. Such models arise frequently in statistical physics to study the interaction between particles. The application of this approach to the problem of network connectivity carries many advantages, which together lead to the novel contributions of our work. These contributions can be summarized as follows:

- 1) We utilize the inhomogeneous cluster expansion model to analyze the effects that boundaries have on connectivity for four important point-to-point link models: single-input single-output (SISO), single-input multiple-output (SIMO), multiple-input single-output (MISO), and multiple-input multiple-output (MIMO). To facilitate this analysis, we define the notion of the *mass of connectivity*, which is an average measure of pair connectedness in a given volume taking boundaries into account.
- 2) We derive diversity and power scaling laws that dictate how boundary effects can be mitigated (to leading order) in confined dense networks. These laws are given for all four of the aforementioned point-to-point link models.
- 3) We corroborate the general theory detailed in [31] by analyzing boundary effects for dense net-

¹This model specifies that connection between two nodes is achieved if and only if the distance between them is at most r , which is some fixed positive number.

²A k -connected network is one that remains fully connected when $k' < k$ point-to-point connections are broken.

³See Fig. 1 for a qualitative illustration of this concept.

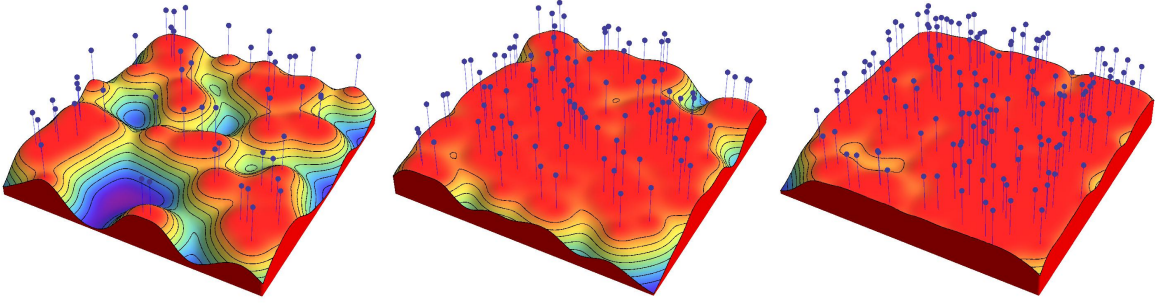


Fig. 1. An illustration of the effects that the boundaries of the network domain have on connectivity. In this example, the network domain is a square of side length $L = 10$ in arbitrary units. The node densities are 0.5, 1, and 1.5, reading left to right. The positions of the nodes for each depicted realization are signified by pins, while the total probability of a new node introduced to the network connecting to any other node is indicated by the contours and shading (blue valleys indicate a low probability of connection while red peaks indicate a high probability). Notice that at high densities, low connection probabilities are concentrated near the corners.

works comprising MIMO point-to-point links confined within a right prism⁴. This example is both instructive and insightful, illustrating the versatility and advantages gained by employing the new cluster expansion theory in network analysis problems.

The rest of the paper is organized as follows. We begin in Section II by giving some preliminary details, which include the point-to-point path loss model and pair-connectedness probabilities for SISO, SIMO, MISO, and MIMO links. In Section III, we give details of the cluster expansion model and derive diversity and power scaling laws for mitigating boundary effects to leading order. We then go one step further by analyzing the connectivity of a network confined in a right prism. Analytical and numerical results for a specific right prism are given in Section IV-E. Finally, we draw some conclusions in Section V.

II. PRELIMINARIES

In this section, we provide preliminary details of the pair connectedness model that we adopt. Specifically, we have that nodes i and j are directly connected with probability $H(d(\mathbf{r}_i, \mathbf{r}_j))$, which we write as $H(\mathbf{r}_{ij})$ or just H_{ij} , where the distance function $d(\mathbf{r}_i, \mathbf{r}_j)$ is non-negative, zero only when $\mathbf{r}_i = \mathbf{r}_j$, and symmetric. We define the pair connectedness probability H_{ij} as the complement of the information outage probability between nodes i and j . This well-understood metric is a natural choice for pair connectedness since it provides fundamental insight into network connectivity behavior, and can even be transformed directly into a unit disk model through appropriate parameter definition if so desired; however, it should also be noted that other pair connectedness models can easily be chosen, such as a model based on the average bit-error rate of a point-to-point link. The outage probability is generally parameterized by the received signal-to-noise ratio (SNR), which in turn is a function of many system parameters as well as the path loss. Consequently, we build our model of pair connectedness starting from a fundamental definition of the path loss model we employ.

A. Path Loss Model and Outage Probability

The received power of an electromagnetic wave decreases with distance like $r^{-\eta}$ where η is an environment-dependent decay parameter. Typically, $\eta = 2$ if propagation occurs in free space, with $\eta > 2$ in cellular/cluttered environments or through walls (see, *e.g.*, [33] and references therein). It follows that the SNR at the receiver (assuming a fixed transmit power P_T and a sufficiently narrow bandwidth⁵) also

⁴A *right prism* is a polyhedron constructed by taking an n -sided polygon as its base, replicating it and translating it in the “vertical” direction, then connecting the corresponding sides. Thus, right prisms are representative of, for example, many room configurations in a building.

⁵Wideband channels sometimes exhibit different path loss behavior, which varies as a function of frequency. Discussion of these channels is beyond the scope of this paper; the interested reader is referred to [34], [35] and references therein.

decays like $r^{-\eta}$. Now, the outage probability for the link between nodes i and j is defined as the probability that the ij link cannot support a given rate R_o in bits per complex dimension, which can be written as

$$P_{ij} = \Pr(\log_2(1 + \text{SNR} \cdot X_{ij}) < R_o)$$

where X_{ij} denotes the random variable signifying the power of the channel between nodes i and j . The pair connectedness probability is simply $H_{ij} = 1 - P_{ij}$, which, after some manipulation, yields

$$H_{ij}(r) = 1 - F_{X_{ij}}(\beta r^\eta) \quad (1)$$

where $F_{X_{ij}}$ is the cumulative distribution function of X_{ij} , and β is a constant – which depends on the frequency of the transmission, the power of the noise process at the receiver, and the transmit power – that defines the length scale. It is important to note that β is inversely proportional to the average received SNR. Finally, we point out that by letting $\eta \rightarrow \infty$, we obtain the unit disk connection model:

$$H_{ij}(r) = \begin{cases} 1, & r < 1 \\ 1 - F_{X_{ij}}(\beta), & r = 1 \\ 0, & r > 1 \end{cases} \quad (2)$$

B. Point-to-Point Link Models

We consider four general point-to-point link models: SISO, SIMO, MISO, and MIMO links. For simplicity, we consider the case where individual channel fading distributions follow a Rayleigh model, and all channels are statistically independent. It follows that X_{ij} has a standard exponential distribution in the SISO case and a chi-squared distribution with $2m$ degrees of freedom in the SIMO/MISO cases (where m is the number of diversity branches employed) [36]. Thus, for SISO links, we have

$$H_{ij}(r) = e^{-\beta r^\eta} \quad (3)$$

and for SIMO/MISO links, we have

$$H_{ij}(r) = \frac{\Gamma(m, \beta r^\eta)}{\Gamma(m)} \quad (4)$$

where $\Gamma(a, x)$ is the upper incomplete gamma function. Equation (4) reduces to the SISO case when $m = 1$.

For MIMO links with n_t transmit antennas and n_r receive antennas, we are mostly concerned with ensuring connectivity is achieved. Thus, we assume beamforming is applied at the transmitter of each node while maximum ratio combining (MRC) is employed at the receiver [37]. For this so-called MIMO MRC channel, the pair connectedness probability becomes

$$H_{ij}(r) = 1 - \kappa_{m,n} \det(\gamma(n - m + i + j - 1, \beta r^\eta))_{ij} \quad (5)$$

where $n = \max(n_t, n_r)$, $m = \min(n_t, n_r)$, $i, j = 1, \dots, m$, $\gamma(a, x)$ is the lower incomplete gamma function, and

$$\kappa_{m,n} = \left(\prod_{i=1}^m \Gamma(n - i + 1) \Gamma(m - i + 1) \right)^{-1}.$$

In order to aid analysis, we will focus on the special case where $m = 2$. This restriction is justified on the basis of pragmatism: indeed, one would envisage that low complexity may be a requirement of nodes operating in dense networks. This is certainly the case in wireless sensor networks where sensors are often powered by batteries [3]. In any case, we maintain some level of generality by not restricting n . For $m = 2$ and general n , we can express H_{ij} as

$$H_{ij}(r) = 1 - nP(n - 1, \beta r^\eta)P(n + 1, \beta r^\eta) + (n - 1)P(n, \beta r^\eta)^2 \quad (6)$$

where $P(n, x)$ is the regularized lower incomplete gamma function. We will use these formulae for H_{ij} in the next section to analyze the probability that a network is connected at the boundary of the confining geometry.

III. PROBABILITY OF FULL CONNECTIVITY

In this section, we develop a novel theory of the probability of full network connectivity in confined geometries through the use of a cluster expansion technique. Cluster expansions are frequently used in statistical mechanics and fluid dynamics to study the interaction between particles. In our application of network connectivity, we first give an overview of the model, then provide details of the first order expansion, which can be used to study connectivity in the high density limit for general pair-connectedness models. For more details on this model, the interested reader is referred to [32]. We then utilize the pair-connectedness functions given in the previous section to analyze the probability of full connectivity at the boundary of the confining geometry to leading order, providing rules that dictate how diversity and power can be scaled to mitigate boundary effects.

A. First Order Cluster Expansion

Consider N randomly distributed nodes with locations $\mathbf{r}_i \in \mathcal{V} \subseteq \mathbb{R}^d$ for $i = 1, 2, \dots, N$ according to a uniform density $\rho = N/V$, where $V = |\mathcal{V}|$ and $|\cdot|$ denotes the size of the set. Here, we use the Lebesgue measure of the appropriate dimension d . We define the average of a quantity as

$$\langle A \rangle = \frac{1}{V^N} \int_{\mathcal{V}^N} A(\mathbf{r}_1, \mathbf{r}_2, \dots, \mathbf{r}_N) d\mathbf{r}_1 d\mathbf{r}_2 \cdots d\mathbf{r}_N.$$

We define some useful notation. Let $S = \{1, 2, 3, \dots, N\}$. A graph $g = (A, L)$ consists of a set $A \subseteq S$ of nodes, together with a collection $L \subseteq \{(i, j) \in A : i < j\}$ of direct links, that is unordered distinct pairs of nodes. As a slight abuse of notation, we write $(i, j) \in g$ to denote that (i, j) is an element of the set of links L associated with the graph g . We write G^A for the set of graphs with nodes in A , and G_j^A for the set with nodes in A and largest connected component (cluster) of size j with $1 \leq j \leq |A|$.

The probability of two nodes being connected or not leads to the trivial identity

$$1 = H_{ij} + (1 - H_{ij}).$$

Multiplying over all links with nodes in a set A expresses the probability of all possible combinations. This can be written as

$$1 = \prod_{i,j \in A; i < j} (H_{ij} + (1 - H_{ij})) = \sum_{g \in G^A} \mathcal{H}_g \quad (7)$$

where

$$\mathcal{H}_g = \prod_{(i,j) \in g} H_{ij} \prod_{(i,j) \notin g} (1 - H_{ij}). \quad (8)$$

The sum in (7) contains $2^{|A|(|A|-1)/2}$ separate terms. Setting $A = S$, this can be expressed as collections of terms determined by their largest cluster, which yields

$$1 = \underbrace{\sum_{g \in G_N^S} \mathcal{H}_g}_{P_{fc}(\mathbf{r}_1, \dots, \mathbf{r}_N)} + \sum_{g \in G_{N-1}^S} \mathcal{H}_g + \cdots + \underbrace{\sum_{g \in G_1^S} \mathcal{H}_g}_{\prod_{i < j} (1 - H_{ij})} \quad (9)$$

For a given configuration of node positions $\mathbf{r}_i \in \mathcal{V}$, assuming that the nodes are pairwise connected with independent probabilities H_{ij} , the first term in equation (9) is the probability of being fully connected $P_{fc}(\mathbf{r}_1, \dots, \mathbf{r}_N)$. The average of this quantity over all possible configurations $P_{fc} = \langle P_{fc}(\mathbf{r}_1, \dots, \mathbf{r}_N) \rangle$ is the overall probability of obtaining a fully connected network and is our desired quantity of interest. Hence, rearranging equation (9) allows us to obtain expressions for P_{fc} in a consistent way while keeping track of correction terms.

Note that in the high density limit of $\rho \rightarrow \infty$, the right hand side of (9) is dominated by the first term, which yields $P_{fc} \approx 1$, and hence the network is fully connected with probability one as expected. The approximation symbol is used here to indicate that first and higher order corrections are being ignored.

The first order approximation is obtained by expanding the second term on the right-hand side of (9) explicitly, taking into account all possible ways of getting an $N - 1$ cluster. Thus the average probability that an N -node network confined in \mathcal{V} is fully connected (to first order) is

$$\begin{aligned}
P_{fc} &\approx 1 - \left\langle \sum_{g \in G_{N-1}^S} \mathcal{H}_g \right\rangle \\
&= 1 - \left\langle \left(\sum_{\varnothing=1}^N \prod_{j \neq \varnothing} (1 - H_{j\varnothing}) \right) \underbrace{\left(\sum_{g \in G_{N-1}^{S \setminus \{\varnothing\}}} \mathcal{H}_g \right)}_{\approx 1} \right\rangle \\
&= 1 - N \left\langle \prod_{j=1}^{N-1} (1 - H_{jN}) \right\rangle \\
&= 1 - \frac{N}{V^N} \int_{\mathcal{V}^N} \prod_{j=1}^{N-1} (1 - H(\mathbf{r}_{jN})) d\mathbf{r}_1 \cdots d\mathbf{r}_N
\end{aligned} \tag{10}$$

where the simplification in the third equality is valid since all nodes are identical, meaning the sum over \varnothing can be factored out.

At this point, we deviate from common practice and assume that the network is *not* translationally symmetric, *i.e.*, the system is inhomogeneous. This ensures that we will include boundary effects in our analysis. Indeed, it turns out that it is not only important to include such effects, but that they *dictate performance* in the limit of high density. This is demonstrated to a large degree through the first order cluster expansion. In particular, we can progress from (10) to obtain

$$\begin{aligned}
P_{fc} &\approx 1 - \frac{N}{V} \int_{\mathcal{V}} \left(1 - \frac{1}{V} \int_{\mathcal{V}} H(\mathbf{r}_{12}) d\mathbf{r}_1 \right)^{N-1} d\mathbf{r}_2 \\
&= 1 - \rho \int_{\mathcal{V}} e^{-\rho \int_{\mathcal{V}} H(\mathbf{r}_{12}) d\mathbf{r}_1} (1 + O(N^{-1})) d\mathbf{r}_2
\end{aligned} \tag{11}$$

in the limit of large N . In fact, this equation was recently given in [30] (eq. (8)), where V was scaled exponentially with ρ , which effectively implies boundary effects are ignored. For our approximation, however, we only require that $V \gg \rho$, or equivalently $V \gg \sqrt{N}$ (cf. [32] for more details on scaling limits of our theory). This is a key difference from previous approaches reported in the literature.

Equation (11) suggests that in the high density limit, the probability of having a single $N - 1$ connected cluster (*i.e.*, having an isolated node) is dominated by nodes that are situated in “hard to connect” regions of the available domain \mathcal{V} . This is because the outer integral in (11) is dominated where the integral in the exponential is small, which occurs at corners, edges, and faces. For nodes located near these geometric effects, the volume in range of the nodes is small.

B. Pair Connectedness and Scaling Laws

Taking a closer look at the integral in the exponent in (11), we see that it effectively defines the *mass of connectivity* for a given pair-connectedness function at \mathbf{r}_2 , and we label it accordingly:

$$M_H(\mathbf{r}_2) = \int_{\mathcal{V}} H(\mathbf{r}_{12}) d\mathbf{r}_1. \tag{12}$$

Indeed, M_H can be studied in detail for different pair-connectedness functions, and power and diversity scaling laws for bounded network connectivity can be gleaned from such an analysis. In the discussion

that follows, it will be understood that M_H is a function of \mathbf{r}_2 , and thus we will refrain from explicitly writing out this relationship for the sake of brevity.

We now incorporate the pair-connectedness functions given in Section II into the model. A common feature of these connection functions is that they decay exponentially with r . This allows us to separate the $d\mathbf{r}_1$ integral in (11) and extract its leading order behavior by supposing that \mathbf{r}_2 is located somewhere on the boundary $\partial\mathcal{V}$ of the network domain $\mathcal{V} \subset \mathbb{R}^d$ [32]. Thus, for a general pair connectedness probability, we have to leading order⁶

$$M_H = \underbrace{\left(\int_0^\infty r^{d-1} H_{ij}(r) dr \right)}_{M'_H} \left(\int d\Omega \right) \quad (13)$$

where $\Omega = 2\pi^{d/2}/\Gamma(d/2)$ is the full solid angle in d dimensions, $\omega = \int d\Omega \in (0, \Omega)$ is the solid angle as seen from \mathbf{r}_2 , and we call M'_H the *homogeneous mass of connectivity* since it characterizes the mass of connectivity in a homogeneous system. Note that the domain of integration in the dr integral is not truncated from above because the integrand is exponentially decaying and, thus, does not contribute significantly to the integral for large arguments (*i.e.*, for nodes located far from the node at \mathbf{r}_2). This approximation clearly demonstrates the influence that boundaries have on connectivity. Specifically, by writing

$$M_H = \delta \Omega M'_H \quad (14)$$

where $\delta = \omega/\Omega \in (0, 1)$, we see that connectivity is dominated from regions that are hard to connect and is controlled by the solid angle available to them. However, we cannot ignore the contribution of M'_H , which will be seen to be useful in determining ways to mitigate a small solid angle contribution.

We now investigate the leading order behavior for the four link models detailed in Section II, placing particular emphasis on how diversity and power control can be used to mitigate boundary effects. Note that in order for us to obtain a more detailed view of boundary effects, we must expand (13) beyond leading order; a discussion to this effect is given in Section IV.

1) *SISO, SIMO, and MISO Link Models*: For SISO, SIMO, and MISO pair connectedness, we have

$$M'_H = \int_0^\infty r^{d-1} \frac{\Gamma(m, \beta r^\eta)}{\Gamma(m)} dr \quad (15)$$

The dr integral can be calculated directly by using the standard integral definition of the incomplete gamma function

$$\Gamma(m, x) = \int_x^\infty t^{m-1} e^{-t} dt$$

and exchanging the order of integration, which eventually yields

$$M'_H = \frac{\Gamma\left(m + \frac{d}{\eta}\right)}{\beta^{\frac{d}{\eta}} d \Gamma(m)}. \quad (16)$$

For uncluttered ($\eta = 2$) d -dimensional networks with point-to-point SISO links, $m = 1$ and we have the simple result

$$M_H = \delta \left(\frac{\pi}{\beta} \right)^{\frac{d}{2}}.$$

Intuitively, one might expect that boundary effects can be mitigated somewhat through the use of diversity (dictated by m in this case). Expanding (16) to leading order as m grows large yields

$$M'_H = \frac{m^{\frac{d}{\eta}}}{\beta^{\frac{d}{\eta}} d} \left(1 + O(m^{-1}) \right). \quad (17)$$

⁶We emphasize that equality is only to leading order here.

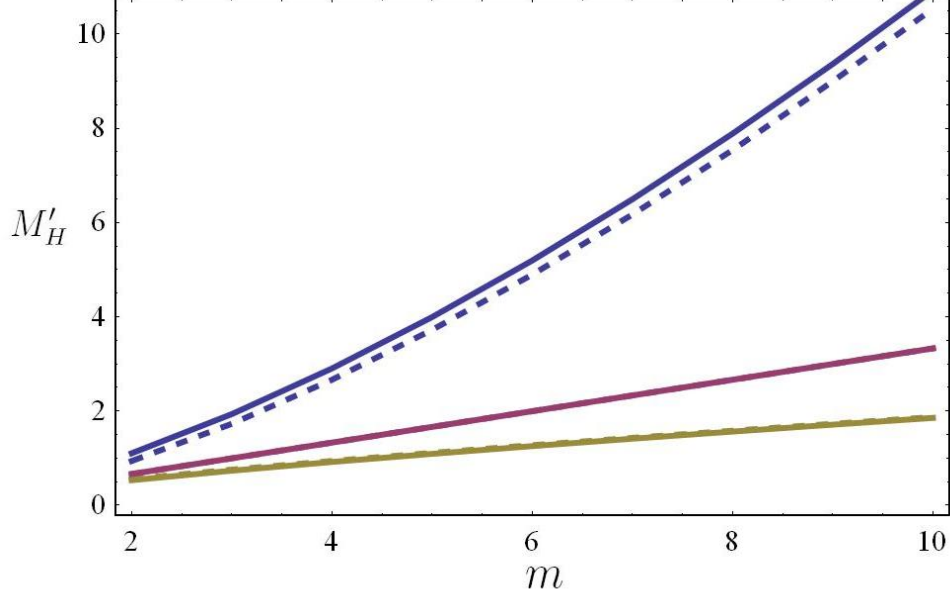


Fig. 2. An illustration of the M'_H scaling law for SIMO/MISO systems. The exact expression given by (16) is represented by solid lines for $d = 3$ and $\eta = 2, 3, 4$ moving from top to bottom. The dashed curves correspond to the leading order behavior.

Thus, we see that although an increase in m results in better connectivity, the rate of increase is highly dependent upon the dimension of the space in which the network resides and the path loss exponent. Indeed, by scaling m , it is possible to obtain a progressive improvement in performance in uncluttered environments ($\eta \approx 2$), whereas cluttered environments ($\eta > 3$) will typically yield diminishing returns. To illustrate this scaling law, we have plotted the exact expression for M'_H along with the leading order term in Fig. 2. Not only is the leading order behavior apparent in this example, but we see that the leading order, in fact, provides an excellent approximation.

As a final note, recall that β is inversely proportional to the average received SNR at a given node. Consequently, it can be seen from (16) that an increase in the transmit power for each node has the same scaling effect as an increase in the diversity order m . However, it should be noted that this analysis is only valid when such an increase is less than exponential relative to the system size, *i.e.*, scaling the transmit power must not counteract the exponential decay in pair connectedness.

The fact that boundary effects can be somewhat mitigated through the appropriate use of diversity and/or power scaling is a powerful conclusion with significant practical implications, particularly since these scaling laws have identical order. For example, some networks may be energy/power constrained (*e.g.*, wireless sensor networks and cognitive networks) whereas others may be constrained by form size (*e.g.*, some vehicular networks). The scaling laws presented here provide engineering insight into how to design networks for a plethora of scenarios.

2) *MIMO Link Models:* We can perform the same analysis for MIMO systems. In this case, we restrict our attention to systems where $m = 2$, for which H_{ij} can be rewritten from (6) into the form

$$H_{ij}(r) = \frac{n\Gamma(n-1, \beta r^\eta) - 2\Gamma(n, \beta r^\eta) + (n-1)^{-1}\Gamma(n+1, \beta r^\eta)}{\Gamma(n-1)} + \frac{\Gamma(n, \beta r^\eta)^2 - \Gamma(n-1, \beta r^\eta)\Gamma(n+1, \beta r^\eta)}{\Gamma(n)\Gamma(n-1)}. \quad (18)$$

Using this form of H_{ij} , we can evaluate M'_H by integrating term by term and using recurrence relations of hypergeometric functions to yield

$$M'_H = \frac{\left(1 - \frac{d}{\eta}\right) \Gamma\left(n - 1 + \frac{d}{\eta}\right)}{\beta^{\frac{d}{\eta}} d \Gamma(n-1)} + \frac{\eta \Gamma\left(2n + \frac{d}{\eta}\right)}{\beta^{\frac{d}{\eta}} d \Gamma(n)^2} \left(\frac{1}{n} F\left(n-1, 2n + \frac{d}{\eta}; n+1; -1\right) - \frac{n-1}{\left(n + \frac{d}{\eta}\right) \left(n - 1 + \frac{d}{\eta}\right)} F\left(n-1 + \frac{d}{\eta}, 2n + \frac{d}{\eta}; n+1 + \frac{d}{\eta}; -1\right) \right) \quad (19)$$

where $F(a, b; c; z)$ denotes the hypergeometric function. The terms involving hypergeometric functions result from integrating the quadratic terms in the expression for H_{ij} given above. Again, the effect of the solid angle defining the volume in range is apparent. Although the expression given above is quite cumbersome and does not necessarily lead to much intuitive insight, we can easily evaluate the approximation for specific values of n . For example, we have for $n = 2$

$$M'_H = \frac{\left(\left(\frac{d}{\eta}\right)^2 + \frac{d}{\eta} + 2 - 2^{-\frac{d}{\eta}}\right) \Gamma\left(\frac{d}{\eta}\right)}{\beta^{\frac{d}{\eta}} \eta}. \quad (20)$$

On the other hand, we can obtain a scaling law in n by noting that for large n , the contributions of the P -functions in (6) are not significant for $\beta r^\eta < n$. Moreover, for $\beta r^\eta > n$, $H_{ij}(r)$ decays exponentially. Thus, we can approximate $H_{ij}(r)$ by a step function with a transition at $r = (n/\beta)^{\frac{1}{\eta}}$. We present an argument for making this approximation in Appendix A. It follows that we can write

$$M'_H = \int_0^{\left(\frac{n}{\beta}\right)^{\frac{1}{\eta}}} r^{d-1} dr + \epsilon(n) = \frac{1}{d} \left(\frac{n}{\beta}\right)^{\frac{d}{\eta}} + \epsilon(n) \quad (21)$$

where the error term is given by

$$\epsilon(n) = \underbrace{\int_0^{\left(\frac{n}{\beta}\right)^{\frac{1}{\eta}}} r^{d-1} (H_{ij}(r) - 1) dr}_{\epsilon_-(n)} + \underbrace{\int_{\left(\frac{n}{\beta}\right)^{\frac{1}{\eta}}}^{\infty} r^{d-1} H_{ij}(r) dr}_{\epsilon_+(n)}. \quad (22)$$

Note that $\epsilon_-(n)$ corresponds to the negative contribution and $\epsilon_+(n)$ is the positive contribution. It remains to determine the order (in n) of the error term. In fact, it can be shown (by way of accurate approximation if not rigorously) that

$$\epsilon(n) = O\left(n^{\frac{d}{\eta} - \frac{1}{2}}\right). \quad (23)$$

A derivation of this result is given in Appendix B. Thus, we can write

$$M'_H = \frac{n^{\frac{d}{\eta}}}{\beta^{\frac{d}{\eta}} d} \left(1 + O\left(n^{-\frac{1}{2}}\right)\right) \quad (24)$$

which is completely analogous to the SIMO/MISO case. This scaling law is illustrated in Fig. 3, where we have plotted the exact expression for M'_H given by (19) along with the leading order term. The leading order growth in n is apparent in this example, but in contrast to the SIMO/MISO case, it is not a good approximation. This results from the fact that the first correction term is $O(n^{-1/2})$ rather than $O(n^{-1})$ as is the case in SIMO/MISO systems. Finally, it is easy to see (by observing (19)) that the same transmit power scaling law holds, *i.e.*, M'_H scales like $\beta^{-\frac{d}{\eta}}$.

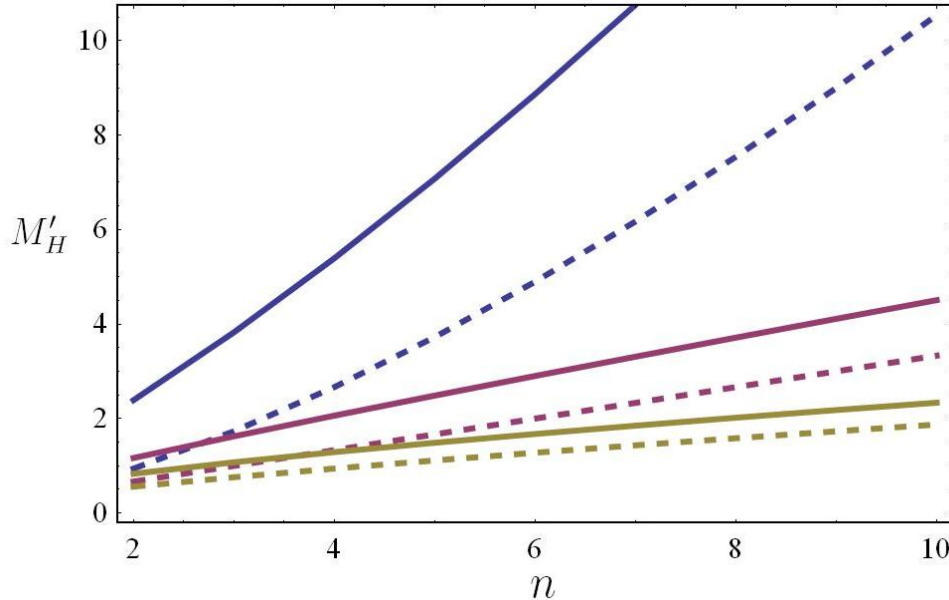


Fig. 3. An illustration of the M'_H scaling law for MIMO systems. The exact expression given by (19) is represented by solid lines for $d = 3$ and $\eta = 2, 3, 4$ moving from top to bottom. The dashed curves correspond to the leading order behavior.

IV. GENERAL FORMULA AND APPLICATIONS TO RIGHT PRISMS

In [32], we developed a general formula for studying the full-connectivity probability in the limit of high density for any network domain. This formula takes the form

$$P_{fc} \approx 1 - \sum_{i=0}^d \sum_{j_i} \rho^{1-i} G_{j_i} V_{j_i} e^{-\rho \omega_{j_i} \int_0^\infty r^{d-1} H(r) dr} \quad (25)$$

where, again, d is the dimension, G_{j_i} is a geometrical factor for each object j_i of codimension i , and V_{j_i} is the corresponding $d - i$ dimensional volume of the object with solid angle ω_{j_i} . In the spirit of this formula, we now derive an expression for P_{fc} by evaluating (11) when the network in question is located in a right prism and the point-to-point links are modeled as uncluttered (*i.e.*, $\eta = 2$) 2×2 MIMO channels. The choice of MIMO point-to-point links for this analysis was taken to demonstrate that our methodology can be applied to reasonably complicated scenarios. Indeed, SISO, SIMO and MISO links can also be analyzed.

The pair connectedness probability for 2×2 MIMO channels with $\eta = 2$ simplifies to

$$H(r) = e^{-\beta r^2} \left(\beta^2 r^4 + 2 - e^{-\beta r^2} \right) \quad (26)$$

where r is the distance between two nodes. To derive P_{fc} in the form of (25), we evaluate the integral (cf. (11))

$$\int_{\mathcal{V}} e^{-\rho \int_{\mathcal{V}} H(\mathbf{r}_{12}) d\mathbf{r}_1} d\mathbf{r}_2 = \int_{\mathcal{V}} e^{-\rho M_H(\mathbf{r}_2)} d\mathbf{r}_2 \quad (27)$$

for each local feature of the geometry⁷. This illustrative example will further show how geometric effects influence connectivity. Moreover, the choice of a right prism as the confining geometry demonstrates the

⁷Here, we have explicitly indicated that the mass of connectivity M_H is dependent upon \mathbf{r}_2 since we will be concerned with first order correction terms.

power and versatility of our theory, particularly since many practical geometries can be well approximated by such a polyhedron.

At this point, it is beneficial and instructive to give an outline of the approach we use to analyze networks confined in right prisms. Our general method is to begin by considering features with the lowest dimension, *i.e.*, corners in this case. We then move to edges, then faces, and finally the bulk of the prism. At each step, we ignore objects of lower dimension since we have accounted for their contribution to connectivity in previous steps. It will be observed that this is a particularly powerful approach when analyzing the effects that the bulk and faces have since the surface (volume) of a right prism is locally equivalent to that of a sphere of the appropriate surface area (volume). We now give details of our analysis, and follow this discussion with a specific example.

A. Corners

For a right prism, each corner is the product of three intersecting planes that can be oriented such that at least one edge connected to its vertex is normal to an adjoining face. This suggests that we should use cylindrical coordinates to perform calculations for this case, where we locate the origin at the vertex and the z -axis is oriented along the edge that connects the two identical polygons.

The distance between two points in cylindrical coordinates is given by

$$d(\mathbf{r}_1, \mathbf{r}_2) = \sqrt{r_1^2 + r_2^2 - 2r_1r_2 \cos(\theta_1 - \theta_2) + (z_1 - z_2)^2}$$

where (r_i, θ_i, z_i) are the coordinates of a node located at \mathbf{r}_i . Thus, in order to evaluate the inner integral of (27) near the corner, we let \mathbf{r}_2 be located near the corner and expand $H(\mathbf{r}_{12})$ near $r_2 = 0$ and $z_2 = 0$, which, to first order, yields

$$\begin{aligned} H(\mathbf{r}_{12}) = & e^{-2\beta(r_1^2+z_1^2)} \left(e^{\beta(r_1^2+z_1^2)} \left(2 + \beta^2 (r_1^2 + z_1^2)^2 \right) - 1 \right) \\ & + 2\beta e^{-2\beta(r_1^2+z_1^2)} \left(e^{\beta(r_1^2+z_1^2)} \left(2 + \beta (r_1^2 + z_1^2) (\beta (r_1^2 + z_1^2) - 2) \right) - 2 \right) \\ & \times (z_1 z_2 + r_1 r_2 \cos(\theta_1 - \theta_2)). \end{aligned} \quad (28)$$

We can now perform the inner integrals in (27) as follows:

$$\begin{aligned} M_H(\mathbf{r}_2) = & \int_0^\infty \int_0^\vartheta \int_0^\infty r_1 H(\mathbf{r}_{12}) dr_1 d\theta_1 dz_1 \\ = & \frac{1}{8\beta} \left(14z_2\vartheta + \frac{23 - \sqrt{2}}{2} \sqrt{\frac{\pi}{\beta}} \vartheta + 7\pi r_2 (\sin \theta_2 - \sin(\theta_2 - \vartheta)) \right) \end{aligned} \quad (29)$$

where ϑ is the angle of the corner with $0 < \vartheta < \pi$. Note that semi-infinite integration is allowed here due to the fact that H is exponentially decreasing but the system size is large⁸. Thus, contributions to the integral at distant boundaries are negligible. Using (29), we are now in a position to calculate the outer integrals of (27), which yields

$$\begin{aligned} \int_{\mathcal{V}} e^{-\rho M_H(\mathbf{r}_2)} d\mathbf{r}_2 = & \iiint r_2 e^{-\rho \int_{\mathcal{V}} H(\mathbf{r}_{12}) d\mathbf{r}_1} dr_2 dz_2 d\theta_2 \\ = & \frac{256\beta^3 \csc \vartheta}{343\pi^2 \rho^3 \vartheta} e^{-\frac{(23-\sqrt{2})\sqrt{\pi}\rho\vartheta}{16\beta^{3/2}}}. \end{aligned} \quad (30)$$

The regions of integration are the same here as for the inner integrals; however, note that the order of integration changes.

All that remains is to enumerate the $2n$ corners for a prism constructed from an n -sided polygon. Each corner is defined by the angle ϑ . For example, a cuboid, which is a right prism formed by replicating and translating a square, has eight corners, all of which have angle $\vartheta = \pi/2$.

⁸In particular, if L denotes the typical length of the geometry, then we require $\sqrt{\beta}L \gg 1$.

B. Edges

Now we consider geometric features of dimension one: edges. Let L be the length of the edge in question. The calculations for this case are also facilitated by the use of cylindrical coordinates, but where the origin is located at the center of the edge. Thus, the corners are located at $\pm L/2$ and the angle of the corner is ϑ . Since we wish to ignore effects from corners, faces, and the bulk, we expand H about $r_2 = 0$ and $z_2 = 0$, which gives (28). Calculating the inner integrals in (27) to first order yields an expression that has $\exp(-\beta L^2/4)$ and $\operatorname{erf}\left(L\sqrt{\beta/2}\right)$ terms. Again, assuming that $\sqrt{\beta}L \gg 1$, we can make the approximations $\exp(-\beta L^2/4) \approx 0$ and $\operatorname{erf}\left(L\sqrt{\beta/2}\right) \approx 1$. It follows that $M_H(\mathbf{r}_2)$ can be evaluated to yield

$$M_H(\mathbf{r}_2) = \frac{1}{4\beta} \left(\frac{23 - \sqrt{2}}{2} \sqrt{\frac{\pi}{\beta}} \vartheta + 7\pi r_2 (\sin \theta_2 - \sin(\theta_2 - \vartheta)) \right) \quad (31)$$

where the integrals are performed over $r_1 \in (0, \infty)$, $\theta_1 \in (0, \vartheta)$, and $z_1 \in (-L/2, L/2)$. The outer integrals in (27) can now be performed to yield

$$\int_{-\frac{L}{2}}^{\frac{L}{2}} \int_0^{\vartheta} \int_0^{\infty} r_2 e^{-\rho M_H(\mathbf{r}_2)} dr_2 d\theta_2 dz_2 = \frac{16L\beta^2 \csc \vartheta}{49\pi^2 \rho^2} e^{-\frac{(23-\sqrt{2})\sqrt{\pi}\rho\vartheta}{8\beta^{3/2}}}. \quad (32)$$

Again, all that remains is to enumerate the $3n$ edges.

C. Faces

For the contribution of the faces to the full-connectivity probability, we employ a *local equivalence* argument that allows us to greatly simplify the analysis. Specifically, we have covered the corner and edge calculations above, and thus we ignore contributions from these features when considering faces. Thus, one can imagine deforming a prism of surface area S into a sphere of the same surface area, the radius R of which is defined by the relation $S = 4\pi R^2$. For a general right prism, the surface area is given by

$$S = 2B + ph$$

where B is the area of the base (*i.e.*, the n -sided polygon), p is the base perimeter, and h is the height. If the base is a regular n -sided polygon with side length s , we have

$$S = \frac{n}{2} s^2 \cot \frac{\pi}{n} + nsh.$$

Thus, this argument allows us to treat any convex right prism that we wish⁹.

Using spherical coordinates along with the fact that the distance between nodes at \mathbf{r}_1 and \mathbf{r}_2 is given by

$$d(\mathbf{r}_1, \mathbf{r}_2) = \sqrt{r_1^2 + r_2^2 - 2r_1 r_2 \cos \theta}$$

where $r_i = |\mathbf{r}_i|$ and $\theta \in [0, \pi]$ is the angle between the nodes, we expand H near the surface of the sphere (*i.e.*, $r_2 = R$) and perform the inner integrals in (27) to obtain

$$\begin{aligned} M_H(\mathbf{r}_2) &= 2\pi \int_0^R \int_0^\pi r_1^2 \sin \theta H(\mathbf{r}_{12}) d\theta dr_1 \\ &= \frac{\pi}{4\beta} \left(\frac{23 - \sqrt{2}}{2} \sqrt{\frac{\pi}{\beta}} + 14(R - r_2) \right) \end{aligned} \quad (33)$$

⁹Convexity is required since we only consider line-of-sight connections between nodes, although small-scale scattering is accounted for through the chosen pair-connectedness models.

where the factor of 2π follows from integration over the azimuthal angle. To arrive at this result, it was assumed that $\sqrt{\beta}R \gg 1$, which allows us to make similar approximations to the error functions of the form $\text{erf}(c\sqrt{\beta}R)$ and exponentials of the form $\exp(-c\beta R^2)$ for some constant $c > 0$ as was done for edges. Furthermore, we have made the additional approximations $c/R \approx 0$ and $c/R^2 \approx 0$. The outer integrals can now be performed to yield (to dominant term in R and ρ)

$$2\pi \int_0^R \int_0^\pi r_2^2 \sin \theta e^{-\rho M_H(\mathbf{r}_2)} d\theta dr_2 = \frac{8\beta R^2}{7\rho} e^{-\frac{(23-\sqrt{2})\pi^{3/2}\rho}{8\beta^{3/2}}}. \quad (34)$$

Generalizing this result to any right prism, *i.e.*, substituting $S = 4\pi R^2$, gives

$$\int_V e^{-\rho M_H(\mathbf{r}_2)} d\mathbf{r}_2 = \frac{2\beta S}{7\pi\rho} e^{-\frac{(23-\sqrt{2})\pi^{3/2}\rho}{8\beta^{3/2}}}. \quad (35)$$

The faces do not need to be enumerated in this case since we have accounted for all faces through the local equivalence argument.

Finally, it is worth mentioning that face contributions can also be calculated in a lengthy manner by using cartesian coordinates. This works well for rectangular sides; however, one must be more careful when considering more general n -sided polygons. In any case, it is straightforward to show for certain simple cases that the proposed approach to the calculation yields identical results to the more complex cartesian approach.

D. Bulk

For the bulk contribution, we apply the same local equivalence argument that was used for the face contributions, but where the expansion in H is performed at $r_2 = 0$. In other words, we consider a sphere of radius R determined by the relation $V = \frac{4}{3}\pi R^3$, where

$$V = Bh$$

is the volume of the right prism containing the network. For a prism constructed from a base that is a regular n -sided polygon with side length s , we have

$$V = \frac{n}{4}hs^2 \cot \frac{\pi}{n}.$$

Expanding H about the origin to first order, we can perform the inner integration to obtain

$$\begin{aligned} M_H(\mathbf{r}_2) &= 2\pi \int_0^\infty \int_0^\pi r_1^2 \sin \theta H(\mathbf{r}_{12}) d\theta dr_1 \\ &= \frac{(23-\sqrt{2})}{4} \left(\frac{\pi}{\beta}\right)^{\frac{3}{2}}. \end{aligned} \quad (36)$$

Finally, the outer integrals can be evaluated to yield

$$2\pi \int_0^R \int_0^\pi r_2^2 \sin \theta e^{-\rho M_H(\mathbf{r}_2)} d\theta dr_2 = V e^{-\frac{(23-\sqrt{2})\pi^{3/2}\rho}{4\beta^{3/2}}}. \quad (37)$$

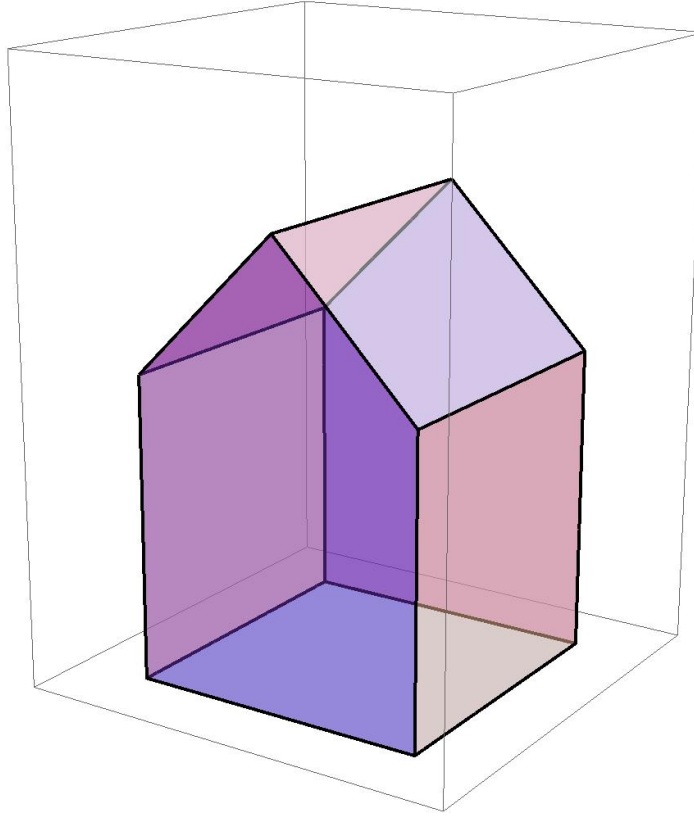


Fig. 4. The “house” prism considered for numerical results. The base is a square of side L , the apex is a right angle, and the total height is $3L/2$.

E. Example: the “House” Prism

We now apply the calculations detailed above to a particular scenario. Specifically, we consider a network comprised of 2×2 MIMO links with $\eta = 2$ operating in a right prism that resembles a typical “house”, as illustrated in Fig. 4. The base of the house is a square of side L . The total height of the prism is $3L/2$, and the apex is right angled. This example somewhat illustrates the versatility of our theory, particularly since most previously published results have considered very simple geometries, such as squares and circles in two dimensions, or cubes and spheres in three dimensions. It should be noted that this is an arbitrary example, and in fact many more complicated geometries can be analyzed with the proposed methodology.

Analysis of the “house” prism is straightforward using the calculations given in the preceding sections. We first identify the different corner angles and count the multiplicities of each. There are ten corners in this prism, six of which have angle $\vartheta = \pi/2$ and four of which have angle $\vartheta = 3\pi/4$. Thus, the following two contributions to the general formula for P_{fc} arise from the corners (cf. (30)):

$$C_1 = 6 \frac{512\beta^3}{343\pi^3\rho^3} e^{-\frac{(23-\sqrt{2})\rho}{32}\left(\frac{\pi}{\beta}\right)^{3/2}} \quad (38)$$

and

$$C_2 = 4 \frac{1024\sqrt{2}\beta^3}{1029\pi^3\rho^3} e^{-\frac{(23-\sqrt{2})3\rho}{64}\left(\frac{\pi}{\beta}\right)^{3/2}}. \quad (39)$$

Next, we perform a similar step for the edges, of which there are fifteen. Thirteen edges are right angled: nine of these have length L while the remaining four have length $L/\sqrt{2}$. The other two edges

TABLE I

CONTRIBUTIONS OF THE VARIOUS GEOMETRICAL FEATURES OF THE “HOUSE” PRISM TO THE GENERAL FORMULA FOR P_{fc} GIVEN BY (25). THE ANGLE $\vartheta = \pi/2$ FOR TYPE-1 CORNER/EDGE CONTRIBUTIONS, AND $\vartheta = 3\pi/4$ FOR TYPE-2 CONTRIBUTIONS.

General Formula Parameter	Corners	Edges	Faces	Bulk
Volume (V_{ji})	1	$L, \frac{L}{\sqrt{2}}$	S	V
Solid Angle (ω_{ji})	ϑ	2ϑ	2π	4π
Geometrical Factor (G_{ji})	$\frac{256\beta^3 \csc \vartheta}{343\pi^3 \vartheta}$	$\frac{16\beta^2 \csc \vartheta}{49\pi^2}$	$\frac{2\beta}{7\pi}$	1

have angle $\vartheta = 3\pi/4$ and length L . Thus, we can write the following two edge contributions to the high density expression for P_{fc} (cf. (32)):

$$E_1 = L \left(9 + 2\sqrt{2}\right) \frac{16\beta^2}{49\pi^2 \rho^2} e^{-\frac{(23-\sqrt{2})\rho}{16} \left(\frac{\pi}{\beta}\right)^{3/2}} \quad (40)$$

and

$$E_2 = 2L \frac{16\sqrt{2}\beta^2}{49\pi^2 \rho^2} e^{-\frac{(23-\sqrt{2})3\rho}{32} \left(\frac{\pi}{\beta}\right)^{3/2}}. \quad (41)$$

For the faces of the prism, we calculate the total surface area to be

$$S = \frac{11 + 2\sqrt{2}}{2} L^2. \quad (42)$$

Thus, using the local equivalence argument presented above, we can substitute this area into (35) to obtain the contribution of all of the faces to P_{fc} . We denote this contribution as F . Similarly, we can take the volume of the prism to be

$$V = \frac{5}{4} L^3. \quad (43)$$

Substituting into (37) yields the bulk contribution to P_{fc} , which we denote by U .

Finally, the general formula is obtained through the summation of all contributions, which yields

$$P_{fc} \approx 1 - \rho (C_1 + C_2 + E_1 + E_2 + F + U). \quad (44)$$

It can easily be seen that this formula has the same structure as (25). In fact, the various contributions to the general formula are outlined in Table I.

Letting $\beta = 1$ and $L = 7$ for simplicity, we have plotted the general formula for this example along with numerical results obtained through simulations in Fig. 5. Furthermore, to illustrate the accuracy of our results at high density, we have plotted the probability of network outage (*i.e.*, $P_{out} = 1 - P_{fc}$) in Fig. 6. In these figures, the two solid curves (reading left to right in both figures) are the numerical and full analytical results (including contributions from all geometrical boundary features). Note that good agreement is achieved at high densities as expected. The left-most dashed curve (red) is the general formula with only a bulk term (*i.e.*, all boundaries are ignored). This curve represents “conventional wisdom”, where boundary effects are neglected, and serves as a benchmark for our results. This benchmark is overly optimistic and should be treated with caution. This is particularly clear in Fig. 6. The next dashed curve (yellow) includes bulk and face contributions. We see that by including even two-dimensional boundary effects, the model is improved significantly. The right-most dashed curve (green) includes bulk, face, and edge contributions, but not corners.

Although these results show that our theory is in excellent agreement with simulations for high densities, they also illustrate the limitations of the theory for low to mid-range densities. However, one notices that, for example, boundaries are not as significant at low densities. Moreover, for mid-range densities, one may only need to consider boundary effects due to faces and/or edges, but not corners, in order to obtain accurate connectivity predictions. This observation can be explained in, perhaps, two ways. Firstly, from a mathematical point of view, our analysis relied heavily on expansions, both near boundaries and at high

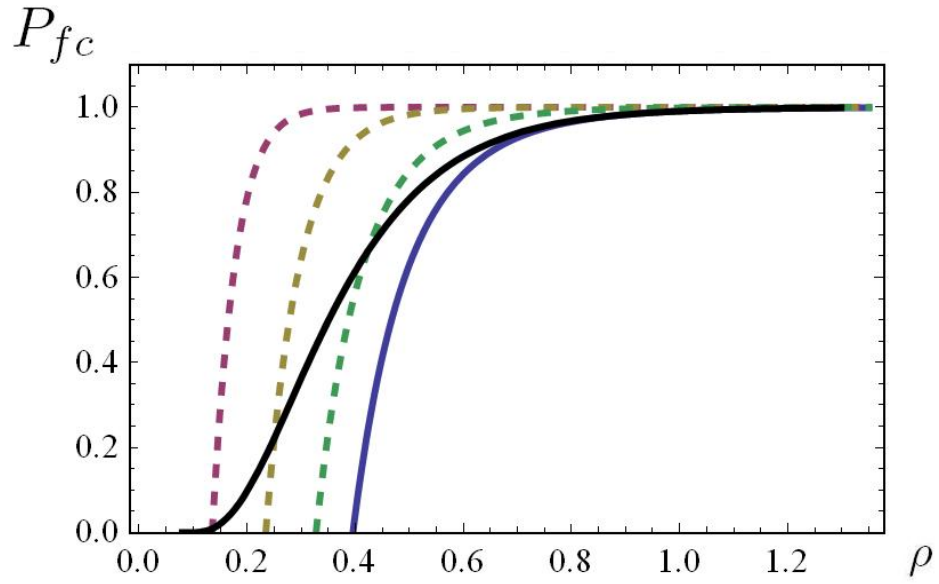


Fig. 5. Analytical and numerical results for the connectivity of a network in a typical “house”. The two solid curves (reading left to right) are the numerical and full analytical results. The left-most dashed curve (red) is the general formula with only a bulk term (*i.e.*, face, edge, and corner terms are ignored). The next dashed curve (yellow) includes bulk and face contributions. The right-most dashed curve (green) includes bulk, face, and edge contributions, but not corners.

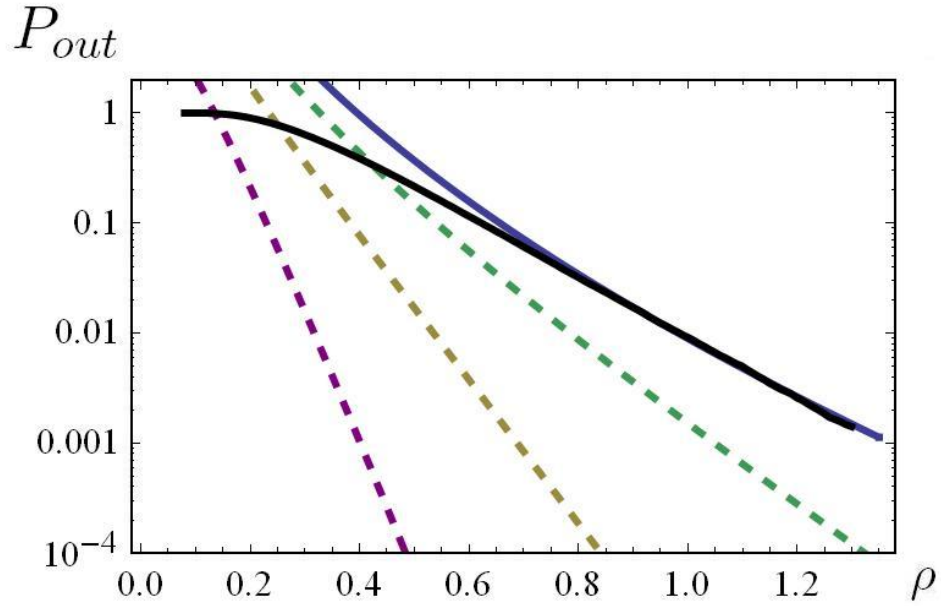


Fig. 6. Analytical and numerical results for the network outage probability in a typical “house”. The labelling of the curves is identical to Fig. 5.

density. To maintain simplicity and tractability, these expansions were typically only to first order. This may be a limitation when considering low to mid-range densities. Secondly, one may intuitively expect that away from the region of high density there is a low probability of a node being located *very* close to a boundary, which of course is where our analysis is valid (again, expansions were taken near boundaries). In any case, our results actually suggest that the theory can be modified somewhat to be valid in regions of low and mid-range densities. This is certainly of interest, and is currently ongoing work.

V. CONCLUSIONS

In this paper, we analyzed the probability of full connectivity for dense networks confined within certain geometries. In contrast to much of the results reported in the literature, we showed that boundary effects should not be ignored, and in fact dictate performance in the high density regime. We built upon our cluster expansion model of full network connectivity, first reported in [31], by adopting four important point-to-point link models for pair connectedness: SISO, SIMO, MISO, and MIMO. This approach allowed us to study the effects that the boundaries of the confining geometry have on practical network connectivity, and led to the derivation of diversity and power scaling laws that dictate how these effects can be mitigated. Finally, we provided a practical example by analyzing the full-connectivity probability of a network comprising MIMO point-to-point links confined within a right prism. This example demonstrated the versatility of our theory in network analysis problems, and we hope that this theory will inspire many researchers in their own problems related to network design and performance analysis.

APPENDIX A

ARGUMENT FOR APPROXIMATING H_{ij} BY A STEP FUNCTION

Let H be given by

$$H(x) = 1 - nP(n-1, x)P(n+1, x) + (n-1)P(n, x)^2.$$

First, consider the case where $x \ll n$. Employing the asymptotic equivalence [38, 8.11.5]

$$P(n, x) \sim \frac{e^{n-x}}{\sqrt{2\pi n}} \left(\frac{x}{n}\right)^n$$

we can write

$$H(x) \sim 1 - \frac{e^{2(n-x)}}{2\pi n} \left(\frac{x}{n}\right)^{2n}$$

and thus $H(x) \rightarrow 1$ as $n \rightarrow \infty$.

Now, consider the case where x is close to but less than n . Let $x = \lambda n < n$ for some $\lambda \approx 1$. Using the asymptotic relations [38, 5.11.3, 8.11.6], we can write

$$P(n, x) = \frac{\gamma(n, x)}{\Gamma(n)} \sim \frac{(n-x)^{-1} x^n e^{-x}}{\sqrt{2\pi n} n^{-\frac{1}{2}} e^{-n}} = \frac{(\lambda e^{1-\lambda})^n}{\sqrt{2\pi n} (1-\lambda)}.$$

But $0 \leq \lambda e^{1-\lambda} < 1$ for $0 \leq \lambda < 1$, and thus $P(n, \lambda n) \rightarrow 0$ for fixed $\lambda < 1$. It follows that $H(x) \approx 1$ for $x < n$ and n large.

Finally, consider the case where x is close to but greater than n . Let $x = \lambda n > n$ for some $\lambda \approx 1$. Now we employ the asymptotic relations [38, 5.11.3, 8.11.7], which give

$$P(n, x) = 1 - \frac{\Gamma(n, x)}{\Gamma(n)} \sim 1 - \frac{(\lambda e^{1-\lambda})^n}{\sqrt{2\pi n} (\lambda - 1)}.$$

But $0 \leq \lambda e^{1-\lambda} < 1$ for $\lambda > 1$, and thus $P(n, \lambda n) \rightarrow 1$ for fixed $\lambda > 1$. It follows that $H(x) \rightarrow 0$ for $x > n$ as $n \rightarrow \infty$. Thus, it is logical to make the stated step function approximation with a transition at $x = n$.

APPENDIX B
ORDER OF THE ERROR TERM

To determine the order of $\epsilon(n)$, we will make use of the expansions [38, 5.11.3]

$$\Gamma(n) \sim \sqrt{2\pi} n^{n-\frac{1}{2}} e^{-n} (1 + O(n^{-1})) \quad (45)$$

and [38, 8.11.12]

$$\Gamma(n, n) \sim \sqrt{\frac{\pi}{2}} n^{n-\frac{1}{2}} e^{-n} (1 + O(n^{-\frac{1}{2}})). \quad (46)$$

Moreover, we have the following identity (which holds for any a , but where the logic behind the proof is given for $a > 0$):

$$\begin{aligned} \frac{\Gamma(n+a, n)}{\Gamma(n)} &= \frac{\Gamma(n+a, n)}{\Gamma(n+a)} \frac{\Gamma(n+a)}{\Gamma(n)} \\ &= \left(\frac{\Gamma(n+a, n+a)}{\Gamma(n+a)} + \frac{1}{\Gamma(n+a)} \int_n^{n+a} t^{n+a-1} e^{-t} dt \right) \frac{\Gamma(n+a)}{\Gamma(n)} \\ &= \frac{1}{2} n^a (1 + O(n^{-\frac{1}{2}})). \end{aligned} \quad (47)$$

Similarly, we have

$$\frac{\Gamma(2n+a, 2n)}{\Gamma(n)^2} = \frac{2^{2(n-1)+a}}{\sqrt{\pi}} n^{a+\frac{1}{2}} (1 + O(n^{-\frac{1}{2}})). \quad (48)$$

We begin by determining the order of

$$\epsilon_+(n) = \int_{(\frac{n}{\beta})^{\frac{1}{\eta}}}^{\infty} r^{d-1} H(r) dr = \frac{1}{\eta \beta^{\frac{d}{\eta}}} \int_n^{\infty} x^{\frac{d}{\eta}-1} \tilde{H}(x) dx$$

where $\tilde{H}(x) = H((x/\beta)^{1/\eta})$. We can rewrite $\tilde{H}(x)$ to yield the following bound on the pair connect-
edness function:

$$\begin{aligned} \tilde{H}(x) &= 2Q(n, x) - Q(n, x)^2 + \frac{x^{2n-1} e^{-2x}}{\Gamma(n)^2} + (1 - Q(n, x)) \frac{(x-n) x^{n-1} e^{-x}}{\Gamma(n)} \\ &\leq \underbrace{2Q(n, x) + \frac{x^{2n-1} e^{-2x}}{\Gamma(n)^2} + \frac{(x-n) x^{n-1} e^{-x}}{\Gamma(n)}}_{\tilde{H}_b(x)}, \quad x \geq n \end{aligned}$$

where $Q(n, x) = 1 - P(n, x) = \Gamma(n, x) / \Gamma(n)$. Now we can write

$$\begin{aligned} \epsilon_+(n) &\leq \frac{1}{\eta \beta^{\frac{d}{\eta}}} \int_n^{\infty} x^{\frac{d}{\eta}-1} \tilde{H}_b(x) dx \\ &= \frac{1}{\eta \beta^{\frac{d}{\eta}} \Gamma(n)^2} \left(2^{1-2n-\frac{d}{\eta}} \Gamma\left(2n-1+\frac{d}{\eta}, 2n\right) \right. \\ &\quad \left. - \Gamma(n) \left(2 \frac{\eta}{d} n^{\frac{d}{\eta}} \Gamma(n, n) + n \Gamma\left(n-1+\frac{d}{\eta}, n\right) - \left(1+2\frac{\eta}{d}\right) \Gamma\left(n+\frac{d}{\eta}, n\right) \right) \right). \end{aligned}$$

Using the expansions given in (45)-(48), it can be shown that this bound behaves like $O(n^{\frac{d}{\eta}-\frac{1}{2}})$.

Considering the negative error term, we have

$$|\epsilon_-(n)| = \frac{1}{\eta \beta^{\frac{d}{\eta}}} \int_0^n x^{\frac{d}{\eta}-1} \tilde{H}_c(x) dx$$

where $\tilde{H}_c(x) = 1 - \tilde{H}(x)$, which behaves like $o(x^{2n-\delta})$ for small $\delta > 0$ as $x \rightarrow 0$, and increases sharply near $x = n$ for large n (see Appendix A). Thus, we propose a semi-rigorous bound on $\tilde{H}_c(x)$ in the form of an exponential with a slope at $x = n$ matched to that of $\tilde{H}_c(x)$, *i.e.*,

$$\tilde{H}_c(x) \leq a_n e^{-b_n(n-x)}$$

where a_n and b_n are constants that may depend on n . Note that $\tilde{H}_c(x)$ increases with x and, thus, has a maximum in the interval $x \in [0, n]$ at $x = n$. Furthermore, $\tilde{H}_c(n)$ decreases with n , so $\tilde{H}_c(x)$ is upper bounded by

$$\tilde{H}_c(n=2) = \frac{2(\cosh 2 - 3)}{e^2}.$$

Furthermore, the slope of $\tilde{H}_c(x)$ at $x = n$ is given by

$$\tilde{H}'_c(n) = \frac{n^n e^{-2n} (2n^n + e^n \gamma(n+1, n))}{\Gamma(n+1)^2}.$$

Matching the slope of the bound at $x = n$ and setting the bound equal to $\tilde{H}_c(n=2)$ at the same point leads to the definitions $a_n = \tilde{H}_c(n=2)$ and $b_n = a_n^{-1} \tilde{H}'_c(n)$.

Making the substitution $t = n - x$ allows us to write

$$|\epsilon_-(n)| \leq \frac{a_n n^{\frac{d}{\eta}-1}}{\eta \beta^{\frac{d}{\eta}}} \int_0^n \left(1 - \frac{t}{n}\right)^{\frac{d}{\eta}-1} e^{-b_n t} dt.$$

By the mean value theorem, we have

$$\begin{aligned} |\epsilon_-(n)| &\leq \frac{a_n \xi_n^{\frac{d}{\eta}-1} n^{\frac{d}{\eta}-1}}{\eta \beta^{\frac{d}{\eta}}} \int_0^n e^{-b_n t} dt \\ &= \frac{a_n \xi_n^{\frac{d}{\eta}-1} n^{\frac{d}{\eta}-1}}{b_n \eta \beta^{\frac{d}{\eta}}} (1 - e^{-b_n n}) \\ &\sim \frac{8\sqrt{2\pi} (\cosh 2 - 3)^2 \xi_n^{\frac{d}{\eta}-1}}{e^4 \eta \beta^{\frac{d}{\eta}}} n^{\frac{d}{\eta}-\frac{1}{2}} \left(1 + O\left(n^{-\frac{1}{2}}\right)\right) \end{aligned}$$

for some $\xi_n \in (0, 1)$. Thus, for $d \geq \eta$, $|\epsilon_-(n)| = O\left(n^{\frac{d}{\eta}-\frac{1}{2}}\right)$.

For $d < \eta$, we have

$$\begin{aligned} |\epsilon_-(n)| &\leq \frac{a_n e^{-b_n n}}{\eta \beta^{\frac{d}{\eta}}} \left(\int_0^1 x^{\frac{d}{\eta}-1} e^{b_n x} dx + \int_1^n x^{\frac{d}{\eta}-1} e^{b_n x} dx \right) \\ &\leq \frac{a_n e^{-b_n(n-1)}}{d \beta^{\frac{d}{\eta}}} + \frac{a_n e^{-b_n n}}{\eta \beta^{\frac{d}{\eta}}} \int_1^n \underbrace{x^{\frac{d}{\eta}-1} e^{b_n x}}_{I_n(x)} dx. \end{aligned}$$

The first term on the right hand side of this inequality goes to zero exponentially with increasing n . Consequently, we focus on the second term. Notice that $I_n(x)$ is convex, with a minimum at $x = \left(1 - \frac{d}{\eta}\right)/b_n$. Moreover, $I_n(1) \rightarrow 1$ as $n \rightarrow \infty$. Thus, the major contribution to the integral $\int_1^n I_n$ occurs near the upper end of the integration region, *i.e.*, $x \approx n$. To make progress, let $y(x) = b_n x - \left(1 - \frac{d}{\eta}\right) \log x$ such that $I_n(x) = e^{y(x)}$ and expand y to first order about $x = n$. This yields the accurate approximation

$$I_n(x) \approx e^{y(n)+y'(n)(x-n)}.$$

We can now integrate easily to obtain

$$\int_1^n I_n(x) dx \approx \frac{e^{1-\frac{d}{\eta}} n^{\frac{d}{\eta}}}{b_n n + \frac{d}{\eta} - 1} \left(e^{b_n n + \frac{d}{\eta} - 1} - e^{b_n - \frac{1-\frac{d}{\eta}}{n}} \right)$$

and thus, to a good approximation, we can write

$$\begin{aligned} |\epsilon_-(n)| &\leq \frac{a_n e^{-b_n(n-1)}}{d\beta^{\frac{d}{\eta}}} + \frac{a_n e^{1-\frac{d}{\eta}} n^{\frac{d}{\eta}-1}}{\eta\beta^{\frac{d}{\eta}} b_n \left(1 + \frac{\frac{d}{\eta}-1}{b_n n}\right)} \left(e^{\frac{d}{\eta}-1} - e^{-b_n(n-1) - \frac{1-\frac{d}{\eta}}{n}} \right) \\ &\sim \frac{8\sqrt{2\pi} (\cosh 2 - 3)^2}{e^4 \eta \beta^{\frac{d}{\eta}}} n^{\frac{d}{\eta}-\frac{1}{2}} \left(1 + O\left(n^{-\frac{1}{2}}\right)\right) \end{aligned}$$

and so we have shown that $\epsilon(n) = O\left(n^{\frac{d}{\eta}-\frac{1}{2}}\right)$.

REFERENCES

- [1] P. Balister, A. Sarkar, and B. Bollobás, “Percolation, connectivity, coverage and colouring of random geometric graphs,” *Handbook of Large-Scale Random Networks*, pp. 117–142, 2008.
- [2] M. Haenggi, J. Andrews, F. Baccelli, O. Dousse, and M. Franceschetti, “Stochastic geometry and random graphs for the analysis and design of wireless networks,” vol. 27, no. 7, pp. 1029–1046, 2009.
- [3] J. Li, L. Andrew, C. Foh, M. Zukerman, and H. Chen, “Connectivity, coverage and placement in wireless sensor networks,” *Sensors*, vol. 9, no. 10, pp. 7664–7693, 2009.
- [4] V. Ravelomanana, “Extremal properties of three-dimensional sensor networks with applications,” *IEEE Trans. Mobile Computing*, vol. 3, no. 3, pp. 246–257, 2004.
- [5] R. Meester and R. Roy, *Continuum Percolation*. Cambridge Univ Pr, 1996, vol. 119.
- [6] T. Hill, “Molecular clusters in imperfect gases,” *The Journal of Chemical Physics*, vol. 23, p. 617, 1955.
- [7] A. Coniglio, U. Angelis, and A. Forlani, “Pair connectedness and cluster size,” *Journal of Physics A: Mathematical and General*, vol. 10, p. 1123, 1977.
- [8] A. Coniglio, U. Angelis, A. Forlani, and G. Lauro, “Distribution of physical clusters,” *Journal of Physics A: Mathematical and General*, vol. 10, p. 219, 1977.
- [9] Y. Chiew and E. Glandt, “Percolation behaviour of permeable and of adhesive spheres,” *Journal of Physics A: Mathematical and General*, vol. 16, p. 2599, 1983.
- [10] G. Stell, “Continuum theory of percolation,” *Journal of Physics: Condensed Matter*, vol. 8, p. A1, 1996.
- [11] I. Glauche, W. Krause, R. Sollacher, and M. Greiner, “Continuum percolation of wireless ad hoc communication networks,” *Physica A: Statistical Mechanics and its Applications*, vol. 325, no. 3–4, pp. 577–600, 2003.
- [12] G. Paschos, P. Mannersalo, and S. Stanczak, “Extending the percolation threshold using power control,” in *Wireless Communications and Networking Conference, 2009. WCNC 2009. IEEE*. IEEE, 2009, pp. 1–6.
- [13] D. Goeckel, B. Liu, D. Towsley, L. Wang, and C. Westphal, “Asymptotic connectivity properties of cooperative wireless ad hoc networks,” vol. 27, no. 7, pp. 1226–1237, Sep. 2009.
- [14] C. Westphal, “A study of the percolation threshold for k-collaborative wireless networks,” in *Communications, 2009. ICC’09. IEEE International Conference on*. IEEE, 2009, pp. 1–6.
- [15] E. Liu, Q. Zhang, and K. Leung, “Connectivity in selfish, cooperative networks,” vol. 14, no. 10, pp. 936–938, Oct. 2010.
- [16] C. Capar, D. Goeckel, and D. Towsley, “Broadcast analysis for large cooperative wireless networks,” *Arxiv preprint arXiv:1104.3209*, 2011, submitted to IEEE Trans. on Information Theory.
- [17] D. Callaway, M. Newman, S. Strogatz, and D. Watts, “Network robustness and fragility: Percolation on random graphs,” *Physical Review Letters*, vol. 85, no. 25, pp. 5468–5471, 2000.
- [18] O. Dousse, P. Thiran, and M. Hasler, “Connectivity in ad-hoc and hybrid networks,” in *INFOCOM 2002. Twenty-First Annual Joint Conference of the IEEE Computer and Communications Societies. Proceedings. IEEE*, vol. 2. IEEE, 2002, pp. 1079–1088.
- [19] H. Ammari and S. Das, “Critical density for coverage and connectivity in three-dimensional wireless sensor networks using continuum percolation,” *IEEE Trans. Parallel and Distributed Systems*, pp. 872–885, 2008.
- [20] M. Franceschetti, O. Dousse, D. Tse, and P. Thiran, “Closing the gap in the capacity of wireless networks via percolation theory,” vol. 53, no. 3, pp. 1009–1018, Mar. 2007.
- [21] G. Mao and B. Anderson, “Towards a better understanding of large scale network models,” *Arxiv preprint arXiv:1012.5723*, 2011, accepted for publication in IEEE/ACM Transactions on Networking.
- [22] P. Gupta and P. Kumar, “Critical power for asymptotic connectivity,” in *Decision and Control, 1998. Proceedings of the 37th IEEE Conference on*, vol. 1. IEEE, 1998, pp. 1106–1110.
- [23] F. Xue and P. Kumar, “The number of neighbors needed for connectivity of wireless networks,” *Wireless networks*, vol. 10, no. 2, pp. 169–181, 2004.
- [24] —, “On the θ -coverage and connectivity of large random networks,” vol. 52, no. 6, pp. 2289–2299, Jun. 2006.

- [25] J. Orriss and S. Barton, "Probability distributions for the number of radio transceivers which can communicate with one another," vol. 51, no. 4, pp. 676–681, Apr. 2003.
- [26] C. Bettstetter, "Failure-resilient ad hoc and sensor networks in a shadow fading environment," in *Proc. IEEE Workshop on Dependability Issues in Ad Hoc Networks and Sensor Networks (DIWANS)*, 2004.
- [27] C. Bettstetter and C. Hartmann, "Connectivity of wireless multihop networks in a shadow fading environment," *Wireless Networks*, vol. 11, no. 5, pp. 571–579, 2005.
- [28] R. Hekmat and P. Van Mieghem, "Connectivity in wireless ad-hoc networks with a log-normal radio model," *Mobile Networks and Applications*, vol. 11, no. 3, pp. 351–360, 2006.
- [29] D. Miorandi, E. Altman, and G. Alfano, "The impact of channel randomness on coverage and connectivity of ad hoc and sensor networks," vol. 7, no. 3, pp. 1062–1072, Mar. 2008.
- [30] G. Mao and B. Anderson, "Connectivity of large scale networks: Emergence of unique unbounded component," *Arxiv preprint arXiv:1103.1991*, 2011, submitted to IEEE Trans. on Mobile Computing.
- [31] J. P. Coon, C. P. Dettmann, and O. Georgiou, "Impact of boundaries on fully connected random geometric networks," *Phys. Rev. E*, to appear, 2012.
- [32] J. P. Coon, C. P. Dettmann, and O. Georgiou, "Full connectivity: corners, edges and faces," *Arxiv preprint arXiv:1201.3123v1*, 2012.
- [33] A. Paulraj, R. Nabar, and D. Gore, *Introduction to space-time wireless communications*. Cambridge University Press, 2003.
- [34] J. Kunisch and J. Pamp, "Measurement results and modeling aspects for the UWB radio channel," in *Ultra Wideband Systems and Technologies, 2002. Digest of Papers. 2002 IEEE Conference on*, 2002, pp. 19–23.
- [35] R. Cepeda, S. C. J. Parker, and M. Beach, "The measurement of frequency dependent path loss in residential los environments using time domain uwb channel sounding," in *Proc. IEEE International Conference on Ultra-Wideband ICUWB 2007*, 2007, pp. 328–333.
- [36] D. Tse and P. Viswanath, *Fundamentals of Wireless Communication*. Cambridge University Press, 2005, available online.
- [37] M. Kang and M. Alouini, "Largest eigenvalue of complex Wishart matrices and performance analysis of MIMO MRC systems," vol. 21, no. 3, pp. 418–426, Apr. 2003.
- [38] F. W. J. Olver, Ed., *NIST Handbook of Mathematical Functions*. Cambridge University Press, 2010.